Surface Characteristics of Hydrosilylated Polypropylene

J. Long, C. Tzoganakis, P. Chen

Department of Chemical Engineering, University of Waterloo, 200 University Avenue West, Waterloo, Ontario, Canada, N2L 3G1

Received 7 May 2002; accepted 13 August 2002

ABSTRACT: Polypropylene containing terminal unsaturation was modified with a hydride-terminated polydimethylsiloxane (PDMS) at three different temperatures through a catalytic hydrosilylation reaction in the melt phase. A comprehensive study on the surface characteristics of hydrosilylated polypropylene (SiPP) was conducted by combining macroscopic thermodynamics, microstructure, and chemical composition measurements. Axisymmetric drop shape analysis–profile (ADSA-P) was used to characterize the surface wettability. The morphology, roughness, and heterogeneity of the surfaces were investigated by the lateral-force mode of atomic force microscopy (LFM). X-ray photoelectron spectroscopy (XPS) was used to quantify the surface chemical composition. LFM images showed that all sample surfaces were rough and heterogeneous on a micrometer scale. XPS analysis showed that the surfaces investigated were complicated in composition and that various oxides existed on the surfaces. The surface wettability was well correlated to the surface microstructure and composition. The surfaces investigated were modeled based on the microstructure observed, and a new scheme was developed to calculate surface free energy and adhesion work. For SiPPs, the lower the reaction temperature, the more PDMS incorporation was observed, the smaller the surface free energy and the work of adhesion, the more hydrophobic the surface, and the lower the permeability. © 2003 Wiley Periodicals, Inc. J Appl Polym Sci 88: 3117–3131, 2003

Key words: structure–property relations; poly(propylene) (PP); ESCA/XPS

INTRODUCTION

Polypropylene (PP) is a major commodity polymer used in the plastics industry. Its low price, good thermal and mechanical properties, chemical inertness, crystallinity, and hydrophobic character are desired in many applications. On the other hand, these features restrict its use in other highly profitable areas that are currently dominated by engineering plastics. Therefore, it is of interest to find a way to chemically alter PP to modify features such as adhesion, chemical reactivity, or hydrophilicity. This would further open a path to the formation of interesting copolymers and the production of compatibilizers for fillers or polymer blends. In these processes, the surface physicochemical properties of PP, such as surface tension (surface free energy), permeability, surface microstructure, and surface chemical composition, are critical. Characterization of these surface properties is therefore of vital importance.

In the present work, PP containing terminal unsaturation was modified with a hydride-terminated polydimethylsiloxane (PDMS) through a catalytic hydrosilylation reaction in the melt phase.[1,2] To determine whether such a modification or hydrosilylation reaction alters the surface features of PP, a comprehensive study on the surface characteristics of hydrosilylated polypropylene (SiPP), degraded PP (DPP), and pure PP is required. In addition, there were several important factors that greatly influenced the hydrosilylation reaction, such as the reaction temperature and the ratio of catalyst to cocatalyst. The influence of the reaction temperature on the hydrosilylation reaction and the surface characteristics of materials obtained will be studied in the present work. The influence of the ratio of catalyst to cocatalyst will be presented in a later article.

The surfaces of the samples obtained through such a catalytic hydrosilylation reaction are complicated. First, they could consist of various chemical species. The possible species include PPs, DPPs, and SiPPs due to partial conversion in the degradation and hydrosilylation reactions. In addition, a variety of oxides also possibly exists on the surface as PP is highly susceptible to oxidation due to the presence of the tertiary hydrocarbon on the carbon atom bonded to the pendant methyl group. Second, these surfaces probably are complicated with respect to surface morphology, molecular orientation, and crystallinity. To characterize such surfaces, comprehensive studies on the macroscopic thermodynamics, the microstructure, and the chemical compositions of these surfaces must be car-

Correspondence to: P. Chen (p4chen@cape.uwaterloo.ca).

Contract grant sponsors: Natural Sciences and Engineering Council of Canada (NSERC); Canadian Foundation for Innovation (CFI); Ontario Graduate Scholarships in Science and Technology (OGSST).

ried out, and multiple powerful techniques have to be employed to study the surface wettability, adhesion, morphology, heterogeneity, and composition.

To identify the wettability or hydrophilicity of a surface, contact-angle measurement is often used. There are three main techniques for measuring the contact angle on flat solid surfaces: the sessile drop (or captive bubble in liquid), the Wilhelmy plate, and the inclined plane methods. A detailed discussion about the three methods can be found elsewhere.[3] In this study, we chose one of the sessile drop methods, axisymmetric drop shape analysis–profile (ADSA-P), which is a novel technique to determine liquid–fluid interfacial tensions and contact angles from the shape of axisymmetric menisci (i.e., from sessile as well as pendant drops).[4] Its basic principle is to fit the experimental drop profile to a theoretical one given by the Laplace equation of capillarity, and the surface tension is generated as a fitting parameter. Other parameters, such as contact angle, drop volume, surface area, and three-phase contact radius, can also be obtained. Details of the methodology and experimental setup can be found elsewhere.[5,6] A more recent development of the ADSA-P application is also available.[7]

As discussed above, the ADSA-P technique can provide the volume of a liquid drop sitting on a solid surface. Thus, the liquid amount penetrating into or through the solid sample and, further, the permeability coefficient can be obtained from the volume change of the drop with time. This, in fact, provides a means of measuring the permeability of polymeric materials. Many methods are available to measure permeability.[8–10] Usually, these methods require a closed system and are costly, and they are applicable only to membranes with high permeability. In this study, the samples are solid SiPP with a thickness of approximately 2.3 mm. The permeability of these samples is rather low. It is not convenient to measure the permeability using conventional methods in an open system. We, therefore, made attempts to use the ADSA-P technique to measure the permeability of the polymers. The experiments were carried out with an open system (real environment) and the results are more significant to applications.

The results of contact-angle measurements obtained by ADSA-P can also be used to quantify other surface thermodynamic properties, such as surface free energy and adhesion work (details are presented in the sections Surface Microscopic Characteristics with LFM and Surface Free Energy below). The two parameters are essential in characterizing a surface as they directly represent the surface property and the interaction between the surface and a fluid.

It is known that the macroscopic surface thermodynamic properties discussed above are determined by the microstructural and chemical compositional features of the surface. Investigations of the surface on a microscale (micrometer or even nanometer scale) are therefore essential for a better understanding of the fundamentals of surface characteristics. In recent years, a powerful tool, atomic force microscopy (AFM), has been used to characterize solid surfaces on both micrometer and nanometer scales. In this study, we chose the lateral-force mode of AFM (LFM) to investigate both the topographic and the friction features of sample surfaces. With LFM, the probe is scanned perpendicular to the direction of its length. The torsion, or twisting, of the cantilever supporting the probe will increase or decrease depending on the frictional characteristics of the surface (greater torsion results from increased friction). It can simultaneously measure and record topographic data and lateral force data. LFM can be extremely useful for identifying surface heterogeneity where the materials have differing frictional characteristics.

To quantitatively determine surface chemical compositions, X-ray photoelectron spectroscopy (XPS) or electron spectroscopy for chemical analysis (ESCA) can be employed as it has become one of the most popular spectroscopic techniques available for surface analysis of polymers. XPS is a surface-sensitive method with a typical information depth of 1–5 nm corresponding to 4–20 atomic or molecular monolayers, determined by the mean free path of electrons. Its strength is the measurement of the chemical-binding state of the surface molecules determined by the so-called chemical shift of the electronic states of the atoms involved. These electronic states are characteristic for the atoms emitting the photoelectrons which are excited by a primary MgKα or monochromatic AlKα radiation. Qualitative and quantitative analysis can be performed using elemental sensitivity factors or comparing areas of the same sample. XPS can be combined with argon sputtering to obtain concentration profiles and information on internal interfaces and layers below the escape depth limit of 1–5 nm. This function will be greatly helpful in this study to determine the surface oxidation layers and the migration of SiPP molecules from the bulk to the surface.

In this article, we present a systematic study using the techniques of ADSA-P, LFM, and XPS to characterize the surfaces of SiPP samples made at three different reaction temperatures and the control samples. The goal is to obtain new insights into the effects of the reaction temperature on the surface characteristics, such as surface wettability, permeability, free energy, roughness, structure, and composition, and then to provide guidelines for the reaction process and the final product application.

EXPERIMENTAL

Production of SiPP

Materials

The PP used in these experiments was a high molecular weight, isotactic material from Montell (KF6100) (Varennes, Canada) having a melt-flow index (MFI) of 3 g/10 min (ASTM D 1238 condition L). Terminal double bonds were generated in the PP material by using a peroxide, 2,5-dimethyl-2,5-(*t*-butylperoxy)hexane (Lupersol 101), from Elf AtoChem (Oakville, Canada). The PP containing the terminal double bonds was hydrosylilated using PDMS (M_w = 60,000 g/mol) and a platinum–divinyltetramethyldisiloxane complex (Karstedt's catalyst) from United Chemical Technologies Inc (Bristol, PA. *t*-Butylhydroperoxide, anhydrous, 5–6*M* in decane, was received from Aldrich (Oakville, Canada), and it was used as a cocatalyst to stabilize and activate the colloid formed between PDMS and the Karstedt's catalyst.[2] Methanol was obtained from VWR (Mississauga, Canada), and toluene (99.5%) for general use was received from BDH (Mississauga, Canada). All chemicals and solvents were used as delivered.

Terminal double-bond generation

PP was degraded to generate the terminal double bonds using 0.5 wt % 2,5-dimethyl-2,5-(*t*-butylperoxy)-hexane (Lupersol 101). The degradation reaction was carried out in the melt phase in a batch mixer (Haake Rheomix 3000) at 200°C for 20 min. Although the bulk of the peroxide was consumed within 2 min, the PP material was kneaded for 20 min to ensure completed peroxide decomposition and complete removal of volatiles.

Hydrosilylation reaction

One hundred ninety-five grams of DPP was added to the batch mixer and melted at various temperatures (160, 180, and 200°C). The desired amount of a platinum catalyst (0.1 mL) and cocatalyst (0.4 mL) was added to 5 g of the liquid PDMS and mixed vigorously. After the platinum colloid was formed, as indicated by the characteristic yellow color of the solution,[11,12] the PDMS mixture was added to the batch mixer with a syringe. Afterward, the mixer was closed with a Teflon stamp and a slight nitrogen overpressure was applied to avoid degradation and oxidation by oxygen.

Cleaning procedure

A thorough cleaning procedure was developed to ensure complete removal of excess PDMS prior to any analysis. This was done by dissolution of the SiPP product from the batch mixer in boiling toluene and subsequent precipitation with methanol. Threefold application of this procedure yielded a clean material that contained only chemically bonded silane.[1,2]

Fourier transform infrared (FTIR) spectroscopy

To quantify the relative amount of PDMS incorporated into DPP in bulk, Fourier transform infrared (FTIR) spectroscopy was employed. Spectra were taken with a Nicolet 520 midrange (500–4000 cm^{-1}) FTIR. The sample material that had been cleaned following the procedure described above was pressed into a thin film in the hot press prior to analysis. Films having a thickness of 0.15 microns were prepared in the hot press at 180–190°C and at 8000 lbs pressure. Incorporation of the siloxane is indicated by the S*i*—O—S*i* absorption at 1100–1030 cm^{-1}, while the shoulder at 888 cm^{-1} is characteristic of the terminal double bonds in the degraded PP.

Samples preparation for surface characterization

Procedure of hot press to produce samples

The samples of SiPP and the control samples (PP and DPP) for the experiments of surface characterization were small disks with a diameter of 25 mm and a thickness of 2.3 mm. These samples were prepared by using a hot press. The procedure included the following six steps: (1) Sample material was placed in the circular cavity of an aluminum mold; (2) the mold containing the sample material was preheated for 2.5 min for SiPP samples and 10 min for the control samples at 200°C; (3) a pressure of 8000 lbs was applied on the mold for 30 s; (4) the press was opened for 2 s for breathing of the sample to remove any air trapped in the mold; (5) the press was closed and pressure (8000 lbs) was applied again for 1 min; and (6) the mold was removed from the hot press and quenched in water.

Surface cleaning

The sample surfaces for contact-angle measurement, AFM imaging, and XPS composition measurement needed be carefully prepared to eliminate contamination. In our experiments, the sample surfaces were first rinsed several times using acetone and double-distilled water, and then the samples were fixed in a sample stand and immerged into deionized water for ultrasonic cleaning. The cleaned samples were dried and placed into a container with a cover. The liquid used for contact-angle measurements was ultrafiltered water with a density of 0.997 g/cm^3 and a surface tension of 72.60 ± 0.09 mJ/m^2.

Contact-angle measurements using ADSA-P

Static contact angles and permeability

To obtain the water permeability of a sample, we needed to know the amount of water penetrating through the sample within a certain period of time. Static sessile drop experiments of ADSA-P could be employed. The experimental procedure was the following: A small drop was first manually deposited onto the surface of the sample. The liquid was added to the drop using a syringe until the contact angle was as large as possible. The static sessile drop generated usually had a radius larger than 3 mm. To eliminate the influence of evaporation, the sample was placed into a sealed chamber saturated with water. A sequence of images of the drop was then recorded and analyzed by the ADSA-P program. As the penetration was slow, a static sessile drop experiment usually lasted for more than 10 h. The penetrating amount and contact area were calculated from the results of the drop volume change and the three-phase contact radius, respectively.

All the experiments of this study were carried out at room temperature (21.3 $\pm$ 0.5°C). For static contact-angle measurements, each experiment was repeated three times, and the results reported are the average values.

Advancing and receding contact angles

Sessile drop contact angle measurements using ADSA-P could be performed as a function of time. A small hole with a diameter of 2 mm was drilled at the center of the disk sample. A Teflon tube with an outer diameter exactly matching the hole size went through the hole from the bottom and reached the top surface. The sample was mounted on a sample stand and the Teflon tube was connected to a motor-driven syringe.[13] An initial drop with a radius of around 1.5 mm was deposited onto the sample surface so as to ensure that the drop was axisymmetric. While using the motor-driven syringe to pump liquid steadily into the sessile drop from below the surface, a sequence of images of the growing drop were captured and the advancing contact angle was obtained. Subsequently, withdrawing the liquid from the drop, the receding contact angle was obtained. The advancing/receding rate used was 0.5–2.5 mm/min (the moving distance of three-phase contact line per unit time). All advancing and receding contact-angle measurements were repeated three times and the results were averaged.

Surface chemical composition measurements with XPS

XPS spectra

XPS measurements were performed with an ESCALAB 250 microprobe system. An AlKα x-rays source (energy 1486.6 eV) was operated at 15 kV and a 20 mA current emission. Energy analysis of the photoelectrons was made with a hemispheric electrostatic analyzer using in the fixed analyzer transmission (FAT) mode with a bandpass equal to 20 eV. For each analyzed specimen, we recorded the wide spectrum (0–1255 eV binding energy) and then the high-resolution spectra of C 1*s*, O 1*s*, Si 2*p*, N 1*s*, and F 1*s* with a scanning step of 0.1 eV. To correct for charge effect, the energy scale was calibrated by taking the C 1*s* binding of C—C species at 285 eV. It should be noted that the XPS probes 2–3 nm of the surface layer with a scanning area of 500 $\times$ 500 μm^2. For each sample, three specimens were measured and the results presented were the average values.

Ar^+ sputtering experiments

Argon ion sputtering was performed with 3 keV energy ions and a 0.36 $\mu A/cm^2$ current beam. XPS spectra were obtained after 5 min of Ar^+ sputtering for all SiPP samples. To obtain a depth profile, an Ar^+ sputtering experiment with an SiPP-200°C specimen was carried out for a longer time and a series of XPS spectra were obtained during the course of sputtering.

Surface microscopic imaging with AFM

The lateral force mode of a commercial AFM (Digital Instruments, Santa Barbara, CA) was employed in the surface microscopy study. Triangular silicon nitride tips were used to obtain topographic and friction images of the sample surfaces. The scanning scales used ranged from 250 nm to 16 μm.

LFM was used to detect the distribution in friction on the sample surfaces. However, since lateral forces could also be applied to the tip by large vertical variations in the topography of the surface, it was difficult to acquire frictional data on rough surfaces. To "separate" the topography information from the frictional information, three images had to be acquired simultaneously for each scan. The first image was the height/topographic image, the second image was the trace friction image, and the third image was the retrace friction image. Subtracting the second image from the third image produced an image on which the topographic information had been removed. In our experiments, the brighter areas on the produced image represented strong friction, whereas the darker areas corresponded to weak friction.

The surface roughness and the roughness factor were obtained from height images. The statistics of surface roughness were derived from ASME B46.1 (Surface Texture: Surface Roughness, Waviness and Lay) available from the American Society of Mechanical Engineers. The definition of surface roughness used in this study, R_a, is the arithmetic average of the

TABLE I
Results of ADSA-P Experiments

Sample	SiPP-160°C	SiPP-180°C	SiPP-200°C	DPP	PP
Initial static contact angle	110 ± 1.5	100 ± 1.3	86 ± 1.0	78 ± 1.8	102 ± 2.0
Permeability coefficient ($\times 10^{-14}$ $m^2.Pa^{-1}$ s^{-1})	1.20 ± 0.04	1.46 ± 0.03	1.86 ± 0.06	10.23 ± 1.43	6.91 ± 0.42
Advancing contact angle (°)	110 ± 3.5	100 ± 1.5	85 ± 2.5	78 ± 2.0	102 ± 1.5
Receding contact angle (°)	No	No	No	No	No
Surface free energy (mJ/m^2)	32.5 ± 0.9	38.8 ± 0.9	47.5 ± 1.2	52.2 ± 1.7	37.6 ± 1.7
Adhesion work (mJ/m^2)	65.1 ± 1.8	77.7 ± 1.8	95.0 ± 2.5	104.4 ± 3.3	75.1 ± 3.5

absolute values of the surface height deviations measured from the mean plane[14]:

$$R_a = \frac{1}{N}\sum_{j=1}^{N} |Z_j| \quad (1)$$

where N is the number of points and Z_j is the height of the jth point. For each scanning scale, five experiments were carried out at different locations of the sample surface, and the mean roughness results were obtained.

The roughness factor, R_f, different from R_a, is defined as the ratio of the three-dimensional surface area to the two-dimensional surface area produced by projecting the surface onto the threshold plane (the threshold plane may be an arbitrarily selected plane):

$$R_f = \frac{\Sigma\ (surface\ area_i)}{\Sigma\ (projected\ area_i)} \quad (2)$$

Both the roughness and the roughness factor were directly obtained by analyzing the topographic images using the software of the AFM.

RESULTS AND DISCUSSION

Static contact angles

The results of the static contact angles are summarized in Table I. Figure 1 shows the results of a typical static contact-angle measurement. From this figure, one can find that the contact angle (θ) and the volume (V) of a sessile drop linearly decrease with time, while the radius (R) of the three-phase contact line remains constant. During the experiment, the environmental chamber, in which liquid drops were formed, was saturated with a large amount of water; thus, liquid evaporation from the sessile drop was eliminated. The volume decrease reflected the amount of the liquid that permeated through/into the polymer samples. This was also verified by our earlier experiments.[15] In those experiments, it was observed that a number of small drops of water appeared on the bottom side of a plate sample after a long experimental time. The linear decrease of volume indicates a constant volume decrease rate for each sample. This rate was used to calculate the penetrating amount of the liquid in the calculation of permeability. From Table I, one notes that the initial contact angles decreased from approximately 110° and 100°, to 86° with the increase of reaction temperature for the three SiPP samples and that DPP has a lowest static contact angle, 78°. The contact angle of PP, 102°, is much higher than that of DPP. These results indicate that the SiPP sample surface became more hydrophobic with a decreasing reaction temperature. The values of initial contact angles are also approximately equal to the advancing contact angles of the corresponding samples (see the section Dynamic Contact Angles below).

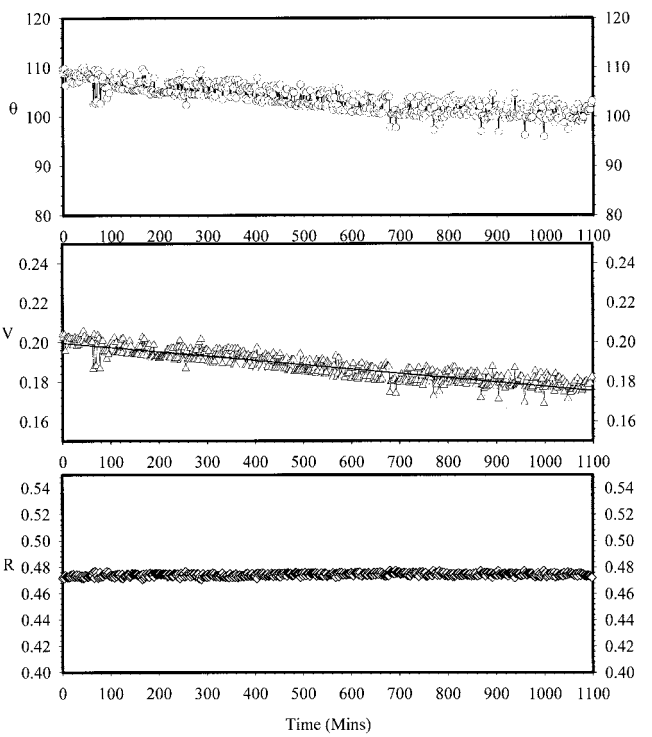

Figure 1 Results of a typical static contact-angle experiment. Sample: SiPP-160°C. Liquid: water. The initial contact angle is about 110°. The volume decreases with the time linearly. The radius of the phase contact line remains constant at 0.472 cm.

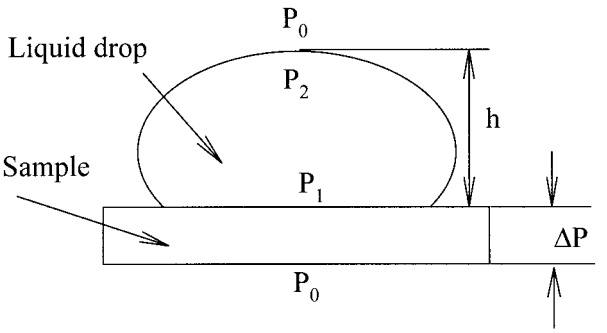

Figure 2 Driving force for the calculation of permeability.

Permeability

To quantify the permeation capability of liquids through the polymers, we employed the permeability coefficient definition as follows[8]:

$$\mathbf{P} = \frac{(penetrating\ amount/time/area)}{(driving\ force/sample\ thickness)} \tag{3}$$

The penetrating amount (volume) per unit time can be calculated directly from the plot of volume versus time as shown in Figure 1. From this figure, one finds that the three-phase contact radius is nearly constant and then the corresponding contact area can be calculated. The driving force is the pressure difference between the two sides of the sample as shown in Figure 2. Here, we assume that the pressure at the bottom side of the sample is the atmospheric pressure P_0. Because of the surface tension, a pressure difference across the liquid surface will exist and can be expressed by the classic Laplace equation of capillarity[16]:

$$P_2 - P_0 = \frac{2\gamma}{R} \tag{4}$$

where γ is the surface tension and R is the radius of the curvature at the apex, which can be obtained from the ADSA-P image analysis. The driving force can thus be obtained:

$$\Delta P = P_1 - P_0 = \frac{2\gamma}{R} + \rho g h \tag{3}$$

where ρ is the density of the liquid; h, the height of the sessile drop; and g, the gravitational acceleration (9.807 m^2/s).

The calculated results of permeability are summarized in Table I. Clearly, the permeability coefficients of the SiPP samples increase with increase of the reaction temperature but they are much lower than those of DPP and PP. The magnitude/value of the permeability coefficient is determined by the interaction between water and the material of the samples. Such interactions will be discussed in the section Work of Adhesion below.

Dynamic contact angles

The advancing and the receding contact angles of water on all the samples were measured. Figure 3 shows a typical set of results of an advancing contact-angle measurement. For all the advancing contact-angle experiments, stable and reproducible advancing contact angles were obtained. The results of dynamic contact angle experiments are summarized in Table I.

In all the advancing contact-angle measurements, similar features (as shown in Fig. 3) are observed. The contact angle increases in the initial stage (e.g., the first 50 s) and then reaches a plateau, which represents the advancing contact angle. For three SiPP samples, their advancing contact angles decrease with an increasing reaction temperature, which indicates that the surface of the sample with a lower reaction temperature is more hydrophobic. This observation will be explained later.

Comparing the advancing contact angles of PP and DPP, one finds that the advancing contact angle of DPP (78°) is much lower than that of PP (102°). This is due to the decrease in molecular weight and the existence of terminal double bonds in DPP. Through a degradation reaction, the long chains of PP molecules

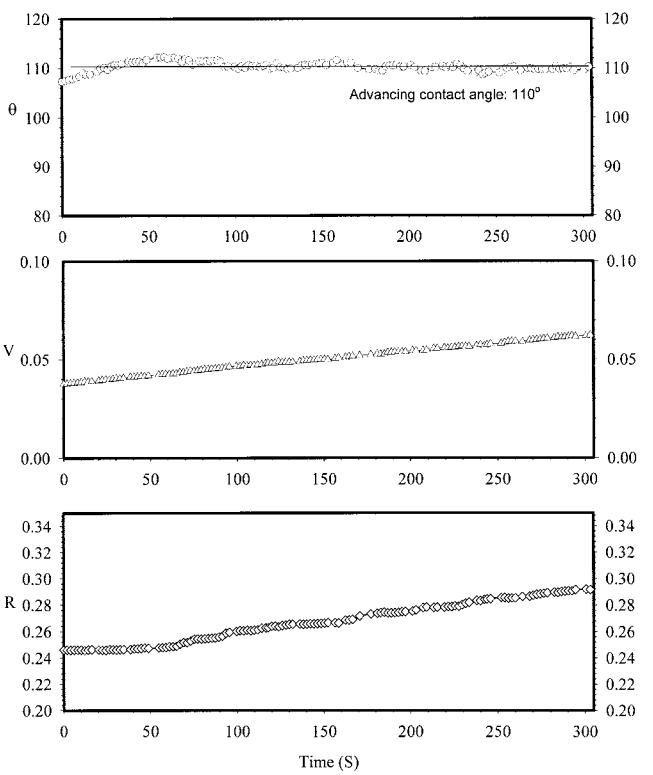

Figure 3 Results of a typical advancing contact-angle measurement. Sample: SiPP-160°C. Liquid: water, Motor rate: 1 step/s. The advancing contact angle is 110°.

were broken and the molecular weight was reduced from 330,000 g/mol (PP) to 160,000 g/mol (DPP). The decrease in molecular weight has a great influence on the properties of PP, for example, the surface microstructure and the molecular orientation. The produced terminal double bonds of C═C are much more hydrophilic than are the C—C bonds. These factors make the surface of a DPP sample more hydrophilic than the surface of a PP sample.

Another point to be noted is that the advancing contact angles of SiPPs are larger than those of DPPs. This can be explained as follows: As we know, the functional groups from PDMS contain the bond of C—Si, which is extremely hydrophobic. When these functional groups were grafted to DPPs through a hydrosililation reaction, the produced SiPPs should be more hydrophobic than the original DPPs. In addition, the difference in hydrophobicity among all the samples indicates that the surface composition may change. This effect is verified by our XPS experiments and will be discussed later.

In comparing the advancing contact angles of water with its initial static contact angles in Table I, one can find that they are approximately identical. This equality arose from the procedure of generating an initial static drop as described in the section Static Contact Angles and Permeability above. The procedure was similar to that of a dynamic sessile drop experiment. Thus, the initial static contact angle should represent the advancing contact angle.

Typical experimental results of a receding contact angle measurement are shown in Figure 4. For all the samples, it is found that the contact angle decreased with time until the drop volume is equal to zero, whereas the three-phase contact radius initially does not change too much with the decrease in drop volume, and at a certain point, it starts to rapidly decrease. From the curve of contact angle, no receding contact angles are observed. This observation is theoretically reasonable and can be explained as follows: The surfaces studied can be considered to be rough and heterogeneous, as one will find later. For such surfaces, either a heterogeneous surface model or a rough surface model[17] can be used to calculate the free energy changes as a function of an instantaneous contact angle. Usually, a number of metastable states exist on a curve describing free-energy changes, and one of these metastable states will correspond to an experimental receding contact angle. However, in some cases, such a metastable state may not exist. That means no receding contact angle will be observed or the receding contact angle is equal to zero.

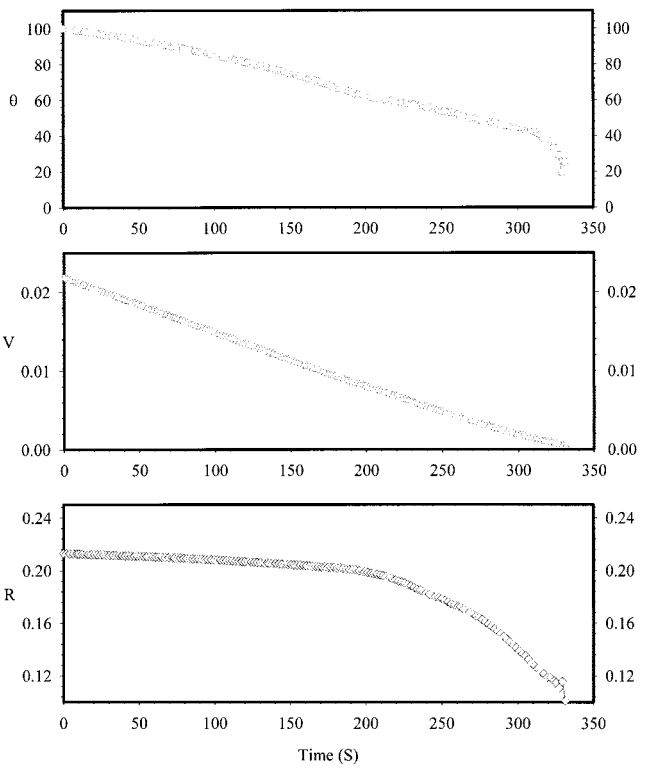

Figure 4 Results of a typical receding contact-angle measurement. Sample: SiPP-180°C. Liquid: water, Motor rate: 2 step/s. The contact angle decreases with decrease of the liquid drop volume. No receding contact angle is observed. Initially, the radius of three-phase contact line remains constant.

Amount of incorporated PDMS in SiPPs through FTIR analysis

The above discussion has revealed the surface hydrophobicity, wettability, and permeability of the SiPPs. It has been found that these surface properties changed with the reaction temperature. To explore how the hydrosilylation reaction and the reaction temperature influence the surface properties of these materials, it is necessary to investigate the amount of PDMS incorporated into DPP and the surface chemical compositions of these materials. In this section, the amount of incorporated PDMS will be discussed, and the next section will present the results of investigating on the surface chemical compositions.

The relative amount of PDMS incorporated into DPP in bulk was determined by FTIR. Thin-film samples of the SiPP material at all three reaction temperatures were analyzed. The relative amount of incorporated PDMS was determined from the height of the absorption peak at 1032 cm^{-1}. The height of this peak was normalized with that of the peak at 841 cm^{-1} (due to the PP backbone) to account for film-thickness variations between the various samples. The results for the samples at 160, 180, and 200°C were 0.298, 0.214, and 0.166, respectively. These results indicate that decreasing the hydrosilylation reaction temperature increases the amount of incorporated PDMS. This is probably due to the slower decomposition of the cocatalyst and, therefore, the longer activation of the PDMS–catalyst complex at lower temperature.[1,2]

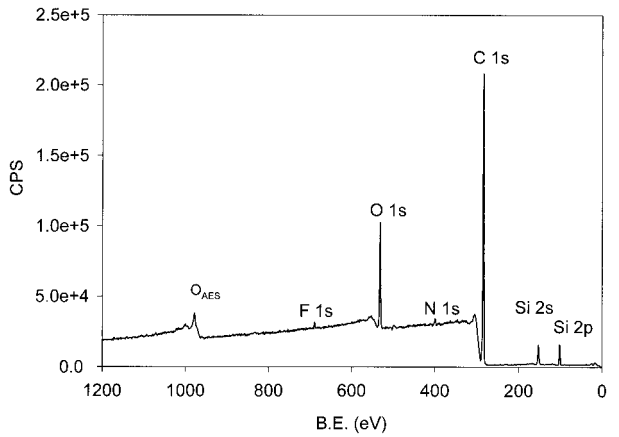

Figure 5 Typical XPS spectrum of a survey scan for the sample of SiPP-200°C. B.E., binding energy; CPS, counts per second.

Surface chemical compositions

The above discussion has revealed the relative amount of incorporated PDMS in SiPPs in bulk. However, the surface chemical composition is more crucial to the surface properties, and the surface chemical composition may differ from that of the bulk due to a possible redistribution of low-energy molecules toward the surface and other factors, for example, surface oxidation. Investigations on the surface compositional features of these materials are needed for further understanding and explaining of the observations in the contact-angle measurements.

Atomic concentrations of surface elements

The surface chemical compositions of all samples were analyzed by XPS. Figure 5 is a typical survey scan. From this figure, it can be seen that the major elements of the surface of SiPP are carbon, oxygen, and silicon, as expected. However, impurities, such as nitrogen and fluorine, exist. Quantitative elemental compositions of a sample surface were obtained by fitting the high-resolution spectrum of each element with components. The results are summarized in Table II. From these results, one can find the following:

Among the three SiPP samples, the atomic concentration of silicon slightly decreases with an increasing reaction temperature but the atomic concentration of oxygen displays an opposite trend. The decreasing trend of surface Si concentration with an increasing reaction temperature is consistent with the relative amount of incorporated PDMS in the bulk. However, the absolute values of the Si atomic concentration, around 6–7%, are significantly different from those in the bulk, which were estimated to be 0.1–0.4% based on the amount of reactants and the approximate PDMS conversion. This indicates that the SiPP molecules migrated from the bulk to the surface. Such migrations were further verified by the sputtering experiments and will be discussed in the following section.

Another point that should be discussed is that the O concentrations are much higher than the Si concentrations on the surfaces of the three SiPP samples. Based on the molecular structure of PDMS,

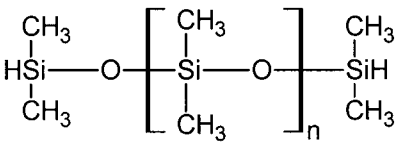

the atomic concentrations of oxygen and silicon from PDMS should be identical. The extra oxygen, found by XPS, on the surfaces of the samples could only come from surface oxidation. As previously mentioned, due to the presence of the pendant methyl group, PP contains tertiary hydrogen atoms, in which the carbon atom covalently bonded to the hydrogen is also bonded to three other carbon atoms. The high probability of reaction with the tertiary hydrogen considerably increases the susceptibility of PP to oxidation. Under normal processing conditions, PP readily undergoes oxidation and oxidative chain scission occurs if it is not stabilized. In addition, the presence of heat

TABLE II
Results of XPS Analysis

	Sample				
Element	SiPP-160°C	SiPP-180°C	SiPP-200°C	DPP	PP
C 1*s*	79.90 ± 0.40	80.37 ± 0.26	78.68 ± 0.85	85.81	88.81
F 1*s*	0.48 ± 0.00	0.24 ± 0.04	0.32 ± 0.01		
N 1*s*	1.19 ± 0.36	1.08 ± 0.23	1.56 ± 0.15	2.25	0.76
O 1*s*	11.44 ± 0.50	11.86 ± 0.27	13.17 ± 0.76	11.85	10.42
Si 2*p*	7.00 ± 0.22	6.45 ± 0.28	6.27 ± 0.09		
O*	4.44 ± 0.46	5.40 ± 0.25	6.90 ± 0.75	11.85	10.42
O*/Si	0.64 ± 0.09	0.84 ± 0.03	1.10 ± 0.13		

All data are atomic concentration (%). For SiPP samples, the results are the average values of three measurements. O*: O not in the bonds of —O—Si. [O*] = [O] − [Si].

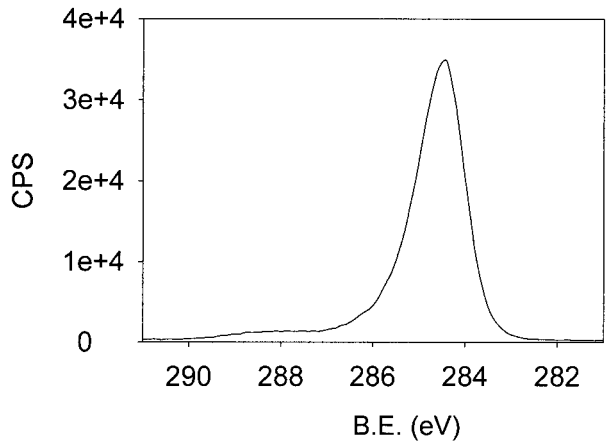

Figure 6 Typical C high-resolution XPS spectrum for the sample of SiPP-200°C.

or metal catalyst residues is believed to speed up oxidation. During oxidation reactions, compounds such as carboxylic acids, lactones, aldehydes, and esters can be produced. These oxides contain various covalent bonds of carbon and oxygen, such as C═O and C—O. In this study, oxidation could occur during the degradation reaction, the hydrosilylation reaction, and/or during the process of samples preparation, in which the materials were exposed to air at 200°C. The atomic concentration of oxygen from oxidation, as indicated by O* in Table II, can be obtained by subtracting the silicon concentration from the total oxygen concentration. As shown in Table II, the O* concentration increases with an increasing reaction temperature for the three SiPP samples. From the XPS analysis results, it can be found that oxidation also occurred to DPP and PP. The O* concentrations of PP and DPP are much higher than those of SiPPs. This probably results from the longer preheating time in preparing the samples of DPP and PP, which is 10 min (3 min for all SiPP samples).

In addition, the presence of oxides on the surfaces can be clearly identified by the high-resolution spectrum of carbon as shown in Figure 6. It is well known that electrons from carbon atoms in such bonds as C═O and C—O will have higher binding energy than that of electrons from carbon atoms of C—C and C—Si bonds. From Figure 6, one finds that the major peak is not axisymmetric and a second peak on the left side can be clearly seen. The area with high binding energy, for example, from 286 to 290 eV, should be attributed to carbon atoms in oxides from surface oxidation.

Relation between surface compositions and surface hydrophobicity

The surface chemical composition results discussed above can be used to explain the increase of surface hydrophilicity with an increasing reaction temperature for SiPP samples. First, as mentioned above, the atomic concentration of silicon slightly decreases with an increasing reaction temperature. From the molecular structure of SiPP, we know that the higher the Si concentration is, the more C—Si bonds on the surface. The C—Si bond is extremely hydrophobic and is the major contributor to surface hydrophobicity for SiPP samples. So, the higher the Si concentration is, the more hydrophobic the surface will be. This implies that the results of atomic concentrations of silicon from XPS are consistent with the observations in the contact-angle measurements. However, it should be noted that the Si concentrations among the three samples only have a slight difference but the variation of surface hydrophobicity is significant. To explain this, one has to consider the presence of surface oxides. These oxides contain hydrophilic functional groups, such as C═O and COO. The more oxides on a surface, the more hydrophilic the surface will be. From the results of the XPS analysis, the atomic concentration of oxygen from oxidation (O*) on the surfaces of SiPP samples increases with an increasing reaction temperature. Considering the opposing effects from Si and O* on the surface hydrophobicity, we calculated the ratio of surface atomic concentrations of O* to Si. As shown in Table II, the ratio of [O*]/[Si] significantly increases with an increasing reaction temperature. This is in good agreement with the increase of surface hydrophilicity as indicated by the results of the contact-angle measurements.

Depth profile of surface compositions

Table III summarizes the results of Ar^+ sputtering experiments. By Ar^+ sputtering, surface molecular

TABLE III
Atomic Concentrations (%) of Elements Before and After Sputtering

	Element					
	Before sputtering			After sputtering for 5 min		
Sample	Si 2*p*	O 1*s*	C 1*s*	Si 2*p*	O 1*s*	C 1*s*
SiPP-160°C	6.90	11.49	81.61	4.43	5.54	90.04
SiPP-180°C	6.42	12.57	81.01	4.45	7.15	88.40
SiPP-200°C	6.68	15.38	77.94	5.48	9.67	84.86

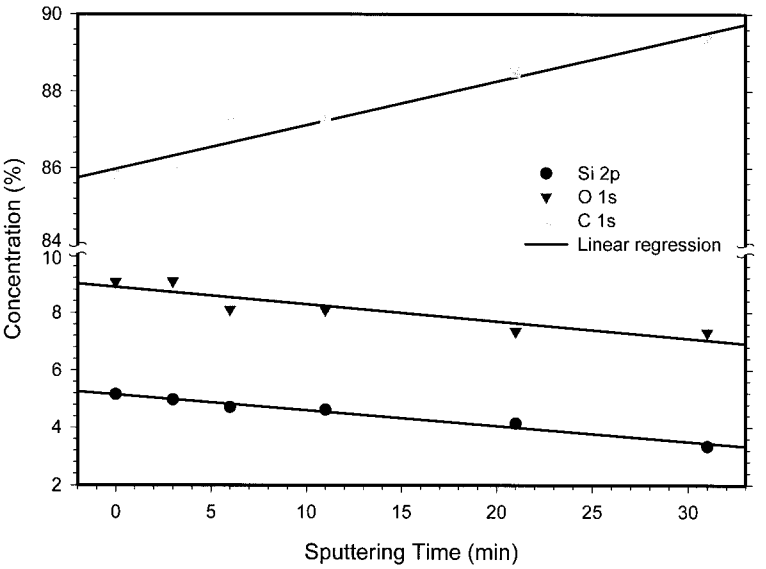

Figure 7 The results of a depth profile. Sample: SiPP-200°C.

layers are removed. The thickness of the removed layers depends on the sputtering time. For 5 min of sputtering, the thickness is estimated to be 3–5 nm. The results obtained after Ar^+ sputtering are the compositions of the freshly produced surfaces. By comparing the results obtained before and after Ar^+ sputtering for all the SiPP samples, it can be found that the atomic concentrations of silicon decrease from 5–6% to 4–5% after Ar^+ sputtering for 5 min. This indicates that the SiPP molecules, which are of low energy, migrate from the bulk to the top surface. From the point of thermodynamics, such a migration is a spontaneous process, as it reduces the surface free energy. In addition, the atomic concentrations of oxygen also decrease. This decrease is around 6%. In subtracting the oxygen from PDMS groups, the extra decrease of around 4% in atomic concentration is due to a decrease in the amount of oxides. This indicates that oxidation occurs most possibly in the top molecular layers.

To further show the variation of concentrations with the surface depth, a depth profile of the surface compositions of SiPP with a reaction temperature of 200°C was obtained by XPS analysis at different sputtering times. As shown in Figure 7, the atomic concentrations of oxygen and silicon linearly decrease with the increase of sputtering time or surface depth.

Surface microscopic characteristics with LFM

The above discussion has well correlated surface hydrophobicity and surface chemical compositions. However, it is well known that an advancing/receding contact angle or contact angle hysteresis, which is defined as the difference between the advancing and the receding contact angle, is directly related to the surface heterogeneity, roughness, and morphology. Investigations on these surface features are still needed for further understanding of the surfaces and correlating the surface wettability/adhesion. In this study, we utilized AFM to explore these features on a micrometer scale. The LFM of AFM was employed.

Surface topographic features

LFM experiments were carried out with eight scan sizes ranging from 0.2, 0.5, 1, 2, 3, 5, and 10 to 16 μm. Here, 16 μm was the maximum scan size that the AFM system could implement and 0.2 μm was the smallest scan size to obtain usable images. Figure 8 shows the typical 3D topographic images of all the samples with a scanning area of 16×16 μm^2. From these images, a similar topographic feature can be observed. All surfaces approximately contain two parallel bumps. The size of the bumps is around 8 μm in width and less than 0.5–1 μm in height. On such a scale, all the surfaces can be described as rough.

To quantify how rough the surfaces are, roughness analysis of the topographic images was carried out. The results are shown in Figure 9. From this figure, one finds that all the samples exhibit approximately identical roughness. This is because the surface structure of samples was determined by the mold surface used in the hot-press process for preparing these samples. Another point that should be noted from this figure is that the roughness increases with an increase of the scanning size. This is due to the size of the bumps on the surfaces. If the scanning size could increase furthermore to cover more bumps on the surfaces, constant values of average roughness should be obtained. These constant values represent the real

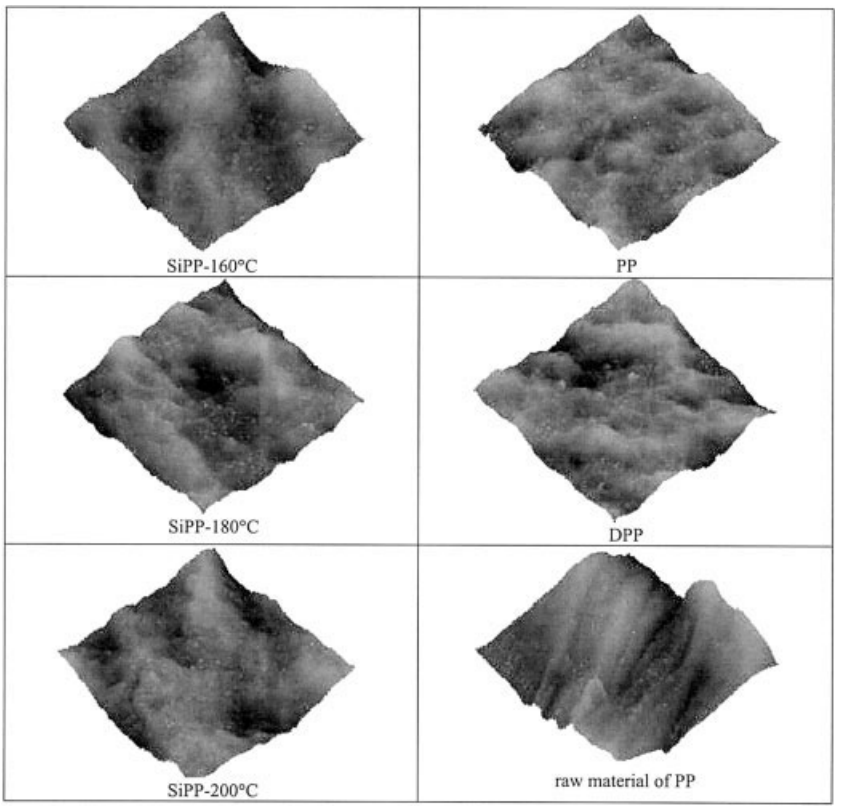

Figure 8 3D topographic images of all the samples. The scanning size is 16 μm. On such a scale, all these surfaces are rough. No clear distinguishable features can be found among these images.

surface roughness. On the scanning size of 16 μm as shown in Figure 9, the surfaces already contain one or two bumps. Therefore, the roughness obtained on such a scale can be considered to be close to the real surface roughness, which is less than 100 nm for all the samples.

Figure 10 shows the results of surface roughness factor. From this figure, it can be seen that there is no significant difference in roughness factors among all the samples and that the roughness factor will reach a certain stable value with an increasing scanning scale. The stable value of the roughness factor at a scanning size of 16 μm is around 1.04 for all the samples. This indicates that the results of the roughness and the roughness factor on the scanning size of 16 μm approximate the real surface properties independent of the scanning size.

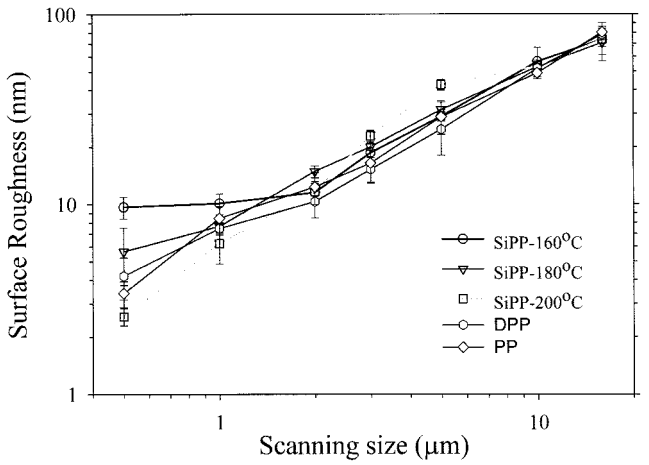

Figure 9 Results of surface roughness as defined in eq. (1).

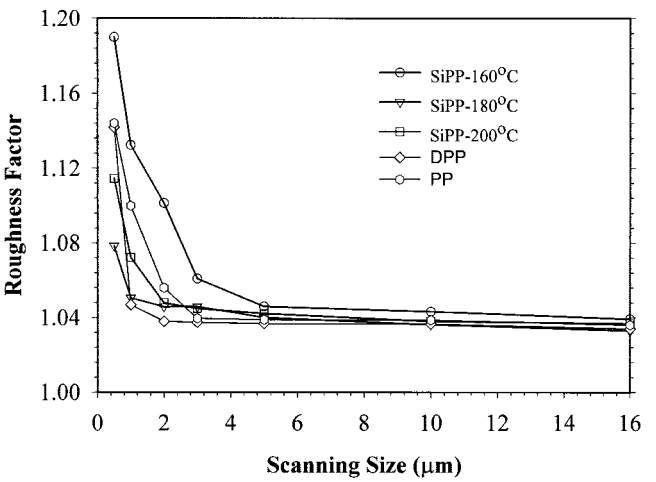

Figure 10 Results of surface roughness factor as defined in eq. (2). After the scan size is larger than 5 μm, there is no significant difference in roughness factor among all the samples.

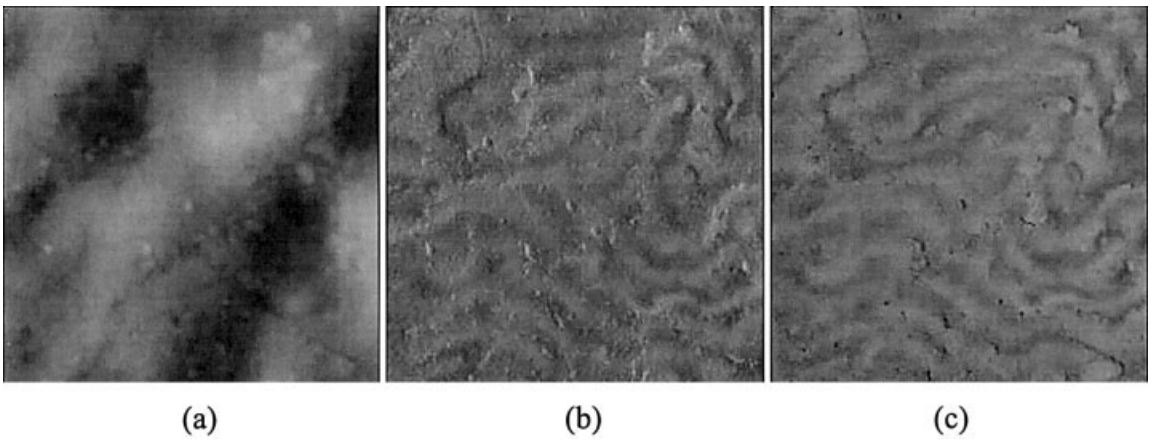

Figure 11 Typical set of images obtained through an LFM scanning. The scan size is 16 μm. Image (a) is the topographic (height) image, (b) the trace friction image, and (c) the retrace friction image. For image (b), the bright areas represent high friction and the dark areas have low friction. On image (c), the information provided is contrary to image (b).

Surface heterogeneity

By using LFM, the topographic and friction features can be obtained simultaneously. Figure 11 shows the images obtained by a typical LFM scanning. In comparing these images, the difference between the topographic image and the friction images is clear. The friction images clearly show that there are different friction domains existing on the surface. The wormlike feature on friction images cannot be seen on the topographic image at all. From the trace and the retrace friction images, a friction image without the influence of topography can be obtained by subtracting the inverted retrace friction image from the corresponding trace friction image. Figure 12 shows such converted friction images for all the samples. The wormlike feature can be seen on all these images, although the regularity and the width of the bright strips are changed. The width of the bright strips is around 0.8–1.5 μm. These surfaces roughly consist of two domains: bright strips and dark valleys, and can be described as being heterogeneous on such a micrometer scale. By AFM bearing analysis, it was found that the bright area on a sample surface takes around 50% of the entire surface area for all the samples.

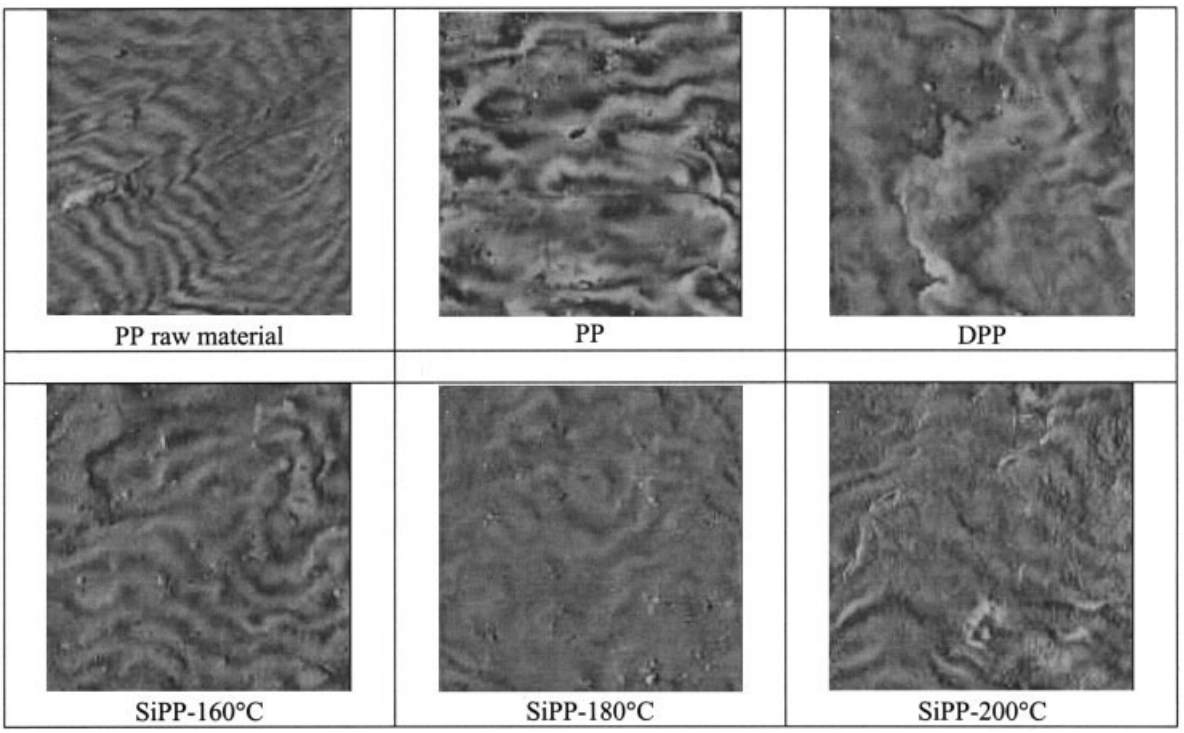

Figure 12 Typical converted friction images for all the samples. The scan size is 16 μm.

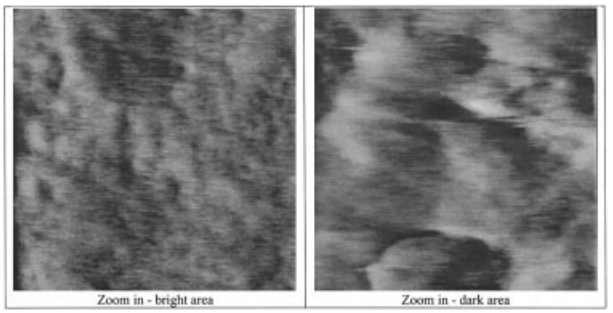

Figure 13 Typical zooming-in images obtained on (left) a bright strip and (right) a dark gap. Sample: DPP. Scanning size: 250 nm.

A friction image reflects the interactions (friction force) between the AFM tip and the sample surface. The different contrasts on a friction image indicate that materials on the surface have differing frictional characteristics, which possibly result from the difference in surface chemical composition, physical structure/state, or even molecular orientation. In the present study, the surfaces of the samples contain various chemical components and the physical structures of these surface materials probably vary, as PP itself is a semicrystalline polymer. Because a silicon nitride tip has a stronger interaction with SiPP molecules, it might be plausible to assume that the bright strips consist mainly of SiPP molecules. In comparing the images in Figure 12, it can be found that the bright strips exist even on the friction images of DPP and PP, which do not have any SiPP molecules. Therefore, the bright strips do not result from SiPP molecules. To further explore the difference between the bright strips and the dark valleys, LFM images were obtained on both locations for each sample as shown in Figure 13. From this figure, the different features between the two images can be clearly observed. On the image from a bright strip (left), there are some small dark patches surrounded by bright areas. On the right image from a dark valley (right), the dark and bright areas are evenly distributed. As a bright area represents high friction compared to a dark area, it is reasonable to speculate that the bright area is amorphous in structure, but the dark area is ordered or possibly crystalline. This is because the contact area between an amorphous surface and a tip is larger than that between a crystalline surface and the tip, and then an amorphous surface will produce stronger friction compared with a crystalline surface. Therefore, it can be assumed that the bright strips contain more amorphous materials than do the dark gaps, which are more organized in molecular structure and possibly contain more crystals.

Surface free energy

Surface free energy is an important thermodynamic property of a solid surface. Its value quantitatively indicates the wettability and hydrophobicity of a surface. Obtaining the surface free energy is essential to the surface characterization. However, current approaches to calculate the surface free energy are available only for ideal surfaces, which are smooth and homogeneous. From the above analysis, it is clear that the surfaces investigated in the present study are both rough and heterogeneous. A new approach was developed for the calculation of surface free energy for such surfaces. Combining the contact-angle measurements and the microstructure investigations, we attempted to model the surfaces and, hence, to calculate the surface free energy as follows:

Based on the topographic features shown in Figure 8, these surfaces can be described first by a model rough surface as shown in Figure 14. This model surface consists of parallel triangular peaks. For the surfaces studied, the height (b) and the width (a) of a peak are around 1 and 8 μm, respectively, and, thus, the angle β is 14°.

In addition, as discussed in the section Surface Heterogeneity above, all the surfaces studied are heterogeneous. From the friction images shown in Figure 12, the surfaces consist of bright strips and dark valleys and thus they can be modeled as an ideal heterogeneous surface containing two materials with intrinsic contact angles θ_{e1} and θ_{e2}, respectively. As shown in Figure 14, this model consists of parallel strips. The dashed and solid segments represent materials one and two, respectively. For the surfaces studied, each strip has the same width, around 1 μm.

For such a heterogeneous and rough surface model, our recent research[18] found the following relation:

$$\theta_A = \theta_C + \beta \tag{6}$$

where θ_A and θ_C are advancing contact angle and the Cassie equilibrium contact angle,[19] respectively. This equation can be used to calculate θ_C. For example, with the advancing contact angle of 102° for PP, we obtained θ_C = 88° for the water/PP system. Then, Young's equation, which is valid for each material, can be employed to calculate surface free energy of each material:

$$\gamma_{lv}\cos\,\theta_{ei} = (\gamma_{sv} - \gamma_{sl})_i \tag{7}$$

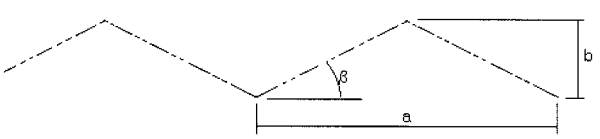

Figure 14 A cross-section view of the ideal rough and heterogeneous surface: (a) the width of a peak; (b) the height. β: the inclination angle. Dashed segments: material 1 with intrinsic contact angle θ_{e1}. Solid segments: material 2 with intrinsic contact angle θ_{e2}.

where γ_{lv}, γ_{sv}, and γ_{sl} are the interfacial tensions of the liquid–vapor, solid–vapor, and solid–liquid, respectively. The subscript i represents material 1 or 2. To find the relation between γ_{sv} and γ_{sl}, Antonow's rule[20] may be applied:

$$\gamma_{sl} = |\gamma_{lv} - \gamma_{sv}| \tag{8}$$

Combining eqs. (7) and (8), the surface free energy of each material can be obtained:

$$(\gamma_{sv})_i = \frac{1 + \cos\theta_{ei}}{2}\gamma_{lv} \tag{9}$$

The surface free energy of a sample can be obtained by averaging all $(\gamma_{sv})_i$:

$$\gamma_{sv} = \sum_i a_i(\gamma_{sv})_i \tag{10}$$

where a_i is the area fraction of material i. In addition, the relation between the Cassie equilibrium contact angle and the intrinsic contact angles can be expressed by the Cassie equation[19]:

$$\cos\theta_C = a_1\cos\theta_{e1} + a_2\cos\theta_{e2} \tag{11}$$

Combining eqs. (9)–(11), the value of the surface free energy of a sample can be obtained by

$$\gamma_{sv} = \frac{1 + \cos\theta_C}{2}\gamma_{lv} \tag{12}$$

The calculated results of the surface free energies are listed in Table I. From these results, one can see that the surface free energy increases with an increase of the reaction temperature for the SiPP samples. It is well known that the larger the surface free energy, the more hydrophilic the surface is. Therefore, we conclude that the higher the reaction temperature, the more hydrophilic the surface is.

Work of adhesion

The surface free energy discussed above is a property of the solid surface itself. However, in some situations, such as the study of permeation, the surface free energy alone is not sufficient to predict the outcome. Another important property, the work of adhesion, is useful. The work of adhesion more directly indicates the interaction between the liquid and the solid. Referring to the definition of the work of adhesion between two phases[16] (eqs. XII-19 and XII-20 in ref. 16), we can define the adhesion work between water and a solid surface in the three-phase system studied as

$$w_{ls} = \gamma_{lv} + \gamma_{sv} - \gamma_{ls} \tag{13}$$

The w_{ls} represents the work necessary to separate a unit area of the liquid–solid interface into a liquid–gas interface and a solid–gas interface. In this study, the surface tension of water γ_{lv} is 72.6 mJ/m^2. The values of γ_{sv} were obtained in the above section. The values of γ_{ls} can be calculated using eq. (8). The computed results of w_{ls} are listed in Table I.

From Table I, it can be seen that, for SiPP samples, the higher the reaction temperature, the higher the work of adhesion and the higher the permeability. Another point found in Table I is that DPP and PP have a much higher permeability than that of the SiPPs. Two important factors influencing the permeability coefficient are the microstructure of the solid and the molecular interaction between the liquid and the solid. These interactions can be represented by the work of adhesion. With increase in the work of adhesion, the interactions between the solid sample and the liquid will increase; thus, the liquid (water) will wet more easily and further penetrate the surface of the sample. For the three SiPP samples, the work of adhesion becomes smaller with decrease of the reaction temperature. Therefore, their permeability coefficients decrease with a decreasing reaction temperature. However, the work of adhesion obtained represents only the surface property, but permeation not only occurs through the surface layers but also through the bulk. Therefore, the effects of the bulk properties of materials on the permeability have to be considered. In the present study, DPP has higher permeability than that of PP. This is because the DPP materials containing C═C double bonds are more hydrophilic than are the PP materials. The reason that the permeability of SiPPs is much less than is the permeability of DPP and PP is because of the presence of PDMS functional groups in SiPPs, which are more hydrophobic. The increasing trend of permeability with an increasing reaction temperature for the three SiPPs is due to the decrease of incorporated PDMS in these materials.

CONCLUSIONS

From the above discussion, the following conclusions can be drawn:

1. A combination of ADSA-P, XPS, and LFM is an effective way for the surface characterization of polymers.
2. Contact-angle measurements and FTIR analysis show that, for SiPPs, the lower the reaction temperature is, the more PDMS was incorporated and the more hydrophobic the surface is.
3. The permeability of the polymers can be obtained by the ADSA-P technique. For SiPPs, the permeability increases with increase of the reaction temperature. The permeability of SiPP is much

less than that of DPP and PP. One of the factors affecting the permeability is the adhesion work between the liquid studied and the solid sample surface. The higher the adhesion work is, the higher the permeability.

4. XPS results show that the surfaces investigated are complicated in composition and that various oxidation states exist on the surfaces. Results of surface chemical composition are in good agreement with the results of the contact-angle measurement. The relative amount of surface oxides to PDMS groups determines the surface wettability/hydrophobicity. For SiPPs, the higher the reaction temperature, the more hydrophilic the surface.
5. The XPS results clearly reveal the redistribution of SiPP molecules from the bulk toward the surface. This redistribution most possibly occurred during the procedure of the samples preparation.
6. All the sample surfaces are rough and heterogeneous on a micrometer scale and no clear topographic difference can be found among all the samples. Wormlike strips were observed on the LFM images, indicating surface heterogeneity, which probably results from the different degrees of the surface crystallinity. Based on the microstructure observations obtained by LFM, the surfaces of samples were modeled by an ideal rough and heterogeneous surface consisting of parallel triangular peaks and alternating composition strips and thus a new scheme was developed to calculate the surface free energy for such rough and heterogeneous surfaces.

Financial support from the Natural Sciences and Engineering Research Council of Canada (NSERC), the Canadian Foundation for Innovation (CFI), and Ontario Graduate Scholarships in Science and Technology (OGSST) is gratefully acknowledged by the authors. The authors gratefully thank Dr. D. K. Sarkar and Prof. T. Leung for their kind assistance in the XPS experiments and analysis and Ms. Y. P. Zhang for preparing the samples and providing details about the materials studied.

References

1. Malz, H.; Tzoganakis, C. Polym Eng Sci 1998, 38, 1976.
2. Tzoganakis, C.; Malz, H. U.S. Patent 6 114 445, Sept. 5, 2000.
3. Erbil, H. Y.; McHale, G.; Rowan, S. W.; Newton, M. I. Langmuir 1999, 15, 7378.
4. Rotenberg, Y.; Boruvka, L.; Neumann, A. W. J Colloid Interf Sci 1983, 93, 169.
5. Lahooti, S.; del Río, O. I.; Cheng, P.; Neumann, A. W. In Applied Surface Thermodynamic; Neumann, A. W.; Spelt, J. K., Eds.; Marcel Dekker: New York, 1966; Vol. 63, p. 441.
6. del Río, O. I.; Neumann, A. W. J Colloid Interf Sci 1997, 196, 136.
7. Long, J.; Chen, P. In 74th Colloid and Surface Science Symposium, Bethlehem, PA, 2000.
8. Comyn, J. Polymer Permeability, 1st ed.; Elsevier: New York, 1985; Chapter 1.
9. Vergnaud, J. M. Liquid Transport Processes in Polymeric Materials, 1st ed.; Prentice-Hall: Englewood Cliffs, NJ, 1991.
10. Vieth, W. R. Diffusion In and Through Polymers, 1st ed.; Hanser: New York, 1991.
11. Lewis, L. N.; Lewis, N. J Am Chem Soc 1986, 108, 7228.
12. Lewis, L. N. J Am Chem Soc 1990, 112, 5998.
13. Kwok, D. Y.; Lin, R.; Neumann, A. W. Colloids Surf A 1996, 116, 63.
14. Digital Instruments, NanoScope® Command Reference Manual (version 4.42).
15. Long, J.; Chen, P. Langmuir 2001, 17, 1965.
16. Adamson, A. W.; Gast, A. P. Physical Chemistry of Surfaces, 6th ed.; Wiley: New York, 1997.
17. Li, D. Q.; Neumann, A. W. In Applied Surface Thermodynamic; Neumann, A. W.; Spelt, J. K., Eds.; Marcel Dekker: New York, 1966; Chapter 3.
18. Long, J.; Chen, P. in preparation.
19. Cassie, A. B. D. Discuss Faraday Soc 1948, 3, 11.
20. Antonow, G. J. Chim Phys 1907, 5, 372.